PHYSICS OF PLASMAS **14**, 057105 (2007)

High planarity x-ray drive for ultrafast shockless-compression experiments[a)]

Raymond F. Smith,[b)] Stephen M. Pollaine, Stephen J. Moon, K. Thomas Lorenz,
Peter M. Celliers, Jon H. Eggert, Hye-Sook Park, and Gilbert W. Collins
Lawrence Livermore National Laboratory, P.O. Box 808, Livermore, California 94550

(Received 4 November 2006; accepted 7 February 2007; published online 4 May 2007)

A spatially planar (Δtime/time $\sim 0.2\%$) longitudinal stress drive extending over millimeter scale lengths is used to shocklessly compress an aluminum sample to a peak stress of 210 GPa over nanosecond time scales. Direct laser irradiation onto the inner wall of an Au halfraum creates an x ray distribution with a near-uniform blackbody temperature of up to 137 eV. The x rays ablate material from a low-Z foil in a region of planarity closely matched to the diameter of the halfraum. The resultant ablatively driven shock is converted into a ramp-stress-wave in a secondary aluminum target through unloading across an intermediate vacuum gap. Higher peak stresses and shorter associated risetimes result from increasing input laser energy. Ramp-compression experiments can provide single shot equation-of-state data close to the isentrope, information on the kinetics of phase transformations, and material strength at high pressures. © *2007 American Institute of Physics*.
[DOI: 10.1063/1.2712450]

I. INTRODUCTION

Recent experiments have demonstrated the production and propagation of high stress ramp-waves that result in quasi-isentropic compression of condensed materials.[1–4] This permits the sampling of thermodynamic space not accessible by near-instantaneous shock compression[5] or static-pressure methods,[6] and ensures a solid state even at very high pressures. Depending on the ramp-wave-loading method, risetimes can be varied between nanoseconds to several microseconds. This capability enables the study of time-dependent material behavior associated with structural changes and deformation in solids subjected to extreme compressions. In these quasi-isentropic compression experiments (ICE) the equation-of-state (EOS) of a material may be determined from Lagrangian sound speed analysis from a multistepped target if an identical ramped stress-wave is applied simultaneously to each of the step samples.[7] Using this technique, the stress-strain response for aluminum (Al-6061) has recently been determined up to a peak stress of 240 GPa when ramp compressed over hundreds of nanoseconds on the Sandia Z-machine.[8]

In previously developed laser-driven ICE an ablatively driven shock in a primary target is transformed into a ramp-compression-wave in a secondary target via unloading followed by stagnation across an intermediate vacuum gap.[1,9,10] Using this direct laser-drive technique peak longitudinal stresses, P_x, of 200 GPa have been obtained. The planarity of the stress drive reported in that work, however, is limited by the performance of the current state-of-the-art laser focal spot smoothing techniques, which precluded their use for EOS measurements.[10] Previous work has demonstrated the potential for generating spatially planar ablative shocks when laser photons are first converted into x rays within a high-Z hohlraum.[11,12]

Here, we have developed a laser-produced x-ray drive to generate ramp-wave loading that was spatially uniform to $\sim 0.2\%$ over 500 μm. This uniform loading ensured that different thicknesses of a multistep target had the same loading history. Ramp-loading risetimes in laser ICE are more than an order of magnitude faster than with other drivers (e.g., pulsed power,[2] gas guns,[3] high explosives[4]) and offer new insights into the rate-dependent response of materials at high levels of compression.

In order to make reliable EOS measurements from a laser ICE a number of criteria need to be satisfied. Each thickness on a multistep target of the material of interest must experience shockless compression. If a compressive shock forms, entropy will be generated and an uncertain amount of target heating will result. In addition, the experimental design should preclude the possibility of target preheat so that the initial temperature and density conditions are well known. The pressure drive needs to be spatially planar such that each step experiences the same loading history. Finally, a detailed error analysis incorporating target and experimental uncertainties coupled with shot-to-shot repeatability is required. One central assumption for all current ramp-wave analysis techniques for extracting EOS information is that the ramp-wave is a simple wave. This implies that there is no rate-dependence in the material properties (e.g., strength) as the propagating ramp-wave steepens during transit.

The layout of this paper is as follows: Section II details the experimental design of laser-ICE EOS targets with experimental results on drive planarity, target preheat and modeling of target dynamics. In Sec. III results describing the energetics of the laser-ICE target are presented.

II. EXPERIMENT

A. Shockless-drive design

A target layout is shown in Fig. 1. Fifteen beams from the Omega laser[13] at 0.35 μm, with a combined energy of up

---

[a)] Paper JI2 1, Bull. Am. Phys. Soc. **51**, 136 (2006).

[b)] Invited speaker.

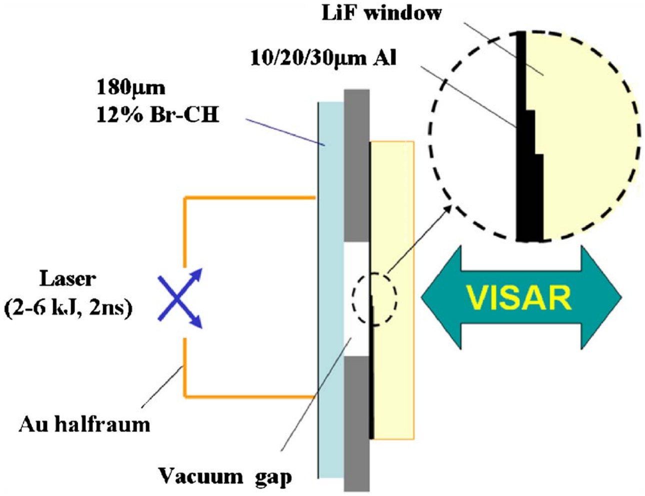

FIG. 1. (Color online) Schematic of indirectly driven laser ICE-EOS target design. Fifteen beams from the Omega laser at 0.35 μm deliver ~5.5 kJ in 2 ns onto the inner walls of an Au halfraum. An ablatively driven shock launched into the reservoir causes it to unload across a vacuum gap and to stagnate upon a stepped Al/LiF target. This stagnation process causes the Al steps to be shocklessly compressed.

to 6 kJ in a 2 ns temporally flat pulse, were focused symmetrically onto the inner walls of an Au "halfraum" (i.e., half of a hohlraum[14]). The halfraum used had 25 μm thick Au walls and the following dimensions: laser entrance hole (LEH): 1.7 mm, diameter: 2.2 mm, length: 1.7 mm. This confined high-Z geometry results in a near-blackbody distribution of thermal x rays with uniform temperature-gradients over a spatial region close to the diameter of the halfraum. For these laser irradiation conditions and halfraum geometry the peak radiation temperature, T_{rad}, was measured with a calibrated array of filtered diodes (Dante spectrometer[15]) to be ~135 eV. The x-ray field within the halfraum launches an ablatively driven shock through a 180 μm thick 12% Br-doped polystyrene reservoir [C_4H_3Br]. The initial region of planarity is expected to approach that of the diameter of the halfraum. Transit through the Br-CH reservoir causes the ablative shock to be hydrodynamically attenuated into a blast-wave which contains no temporal information pertaining to the initial laser drive. The bromine dopant absorbs high energy Au *M*-band x rays (~2–5 keV) generated within the halfraum which otherwise could preheat the Al step sample. After breakout from the rear surface, shock heating and momentum cause the Br-CH plasma to unload across a ~400 μm vacuum-gap and pile-up against a multistep aluminum sample launching a ramped-stress wave. The temporal profile of this compression wave may be shaped by varying the size of the vacuum-gap, the density of the reservoir or the temperature within the halfraum.

Due to the increase of sound speed with increasing pressure the ramp-stress-wave will eventually steepen up into a shock within the Al sample. This would result in a near instantaneous jump in entropy and off-isentropic compression (and possible target melting) would ensue. This shock-up distance is estimated by modeling the target and irradiation conditions with a 1D hydrocode. The maximum Al thickness is therefore designed to be less than the calculated shock-up thickness. In the experiments described here we used 10/20/30 μm Al steps coated onto a LiF window. To make these samples, the Al was coated directly onto a 500 μm thick stepped LiF window using electron-beam deposition at a growth temperature of 425 K and was then later micromachined to ensure all surfaces were parallel. The thickness uniformity across the sample was determined with white light interferometry to be less than 1% (Δthickness/thickness).

As the stress wave reaches the back surface of the Al, it begins to accelerate into the well impedance-matched LiF window. The interface velocity history, u, is recorded with a line-imaging velocity interferometer (VISAR: velocity interferometer system for any reflector) with two channels set at different sensitivities.[16] Figure 2(a) shows a typical streak camera output of the VISAR for an Al/LiF target. The VISAR gives one-dimensional (1D) spatial resolution of 5 μm over a 500 μm field of view across the Al steps. The time-resolved fringe movement recorded by a streak camera is linearly proportional to the velocity of the reflecting surface, which in this case is the Al-LiF interface. The temporal resolution is 50 ps over a 30 ns time window. The velocity per fringe is 1.105 km s^{-1} and we detect fringe position to 5% of a fringe.

The measured interface velocity is very close to the *in situ* particle velocity due to the comparable mechanical impedance of LiF and Al. Furthermore, the refractive index of LiF depends linearly on density in this regime, so the index correction for the velocity calibration is trivial.[17] Figure 2(b) shows representative particle-velocity histories for each of the 10, 20, and 30 μm thick steps. For all Al/LiF samples, we observed a low amplitude precursor similar to the elastic precursor in shock experiments.[18] This velocity plateau corresponds to longitudinal stress, $P_x \sim 2.7$ GPa, which is significantly higher than the reported Hugoniot Elastic Limit (HEL) for pure Al (~0.4 GPa) on millimeter-scale thick targets[18] and 17 times higher than quasistatic tensile measurements on the same material used here.

The dynamics of the unloading solid density Br-CH foil dictates the temporal shape of the initial ramp-compression wave launched into the aluminum. As observed in Fig. 2(b) the ramp-compression wave hydrodynamically steepens into a shock for $u < 1$ km/s after propagating 30 μm in the Al sample. Softening out the foot on the compression-wave would increase this shock-up distance and allow for larger step heights and hence smaller error bars in EOS measurements. Recent work[19] has demonstrated that the use of a graded density at the reservoir/vacuum-gap interface lengthens the shock-up distance.

B. Halfraum closure

Arriving ~10 ns after the peak of the ramp-wave is a spherically shaped compressive shock [Fig. 2(a)]. To understand the origin of this spherical shock we simulated the halfraum physics with a two-dimensional (2D) radiation-hydrodynamics code, LASNEX.[20] Shown in Fig. 3(a) is a radial cutout view of the halfraum at three discrete times (0, 10, and 20 ns) relative to the time the laser energy turns on,

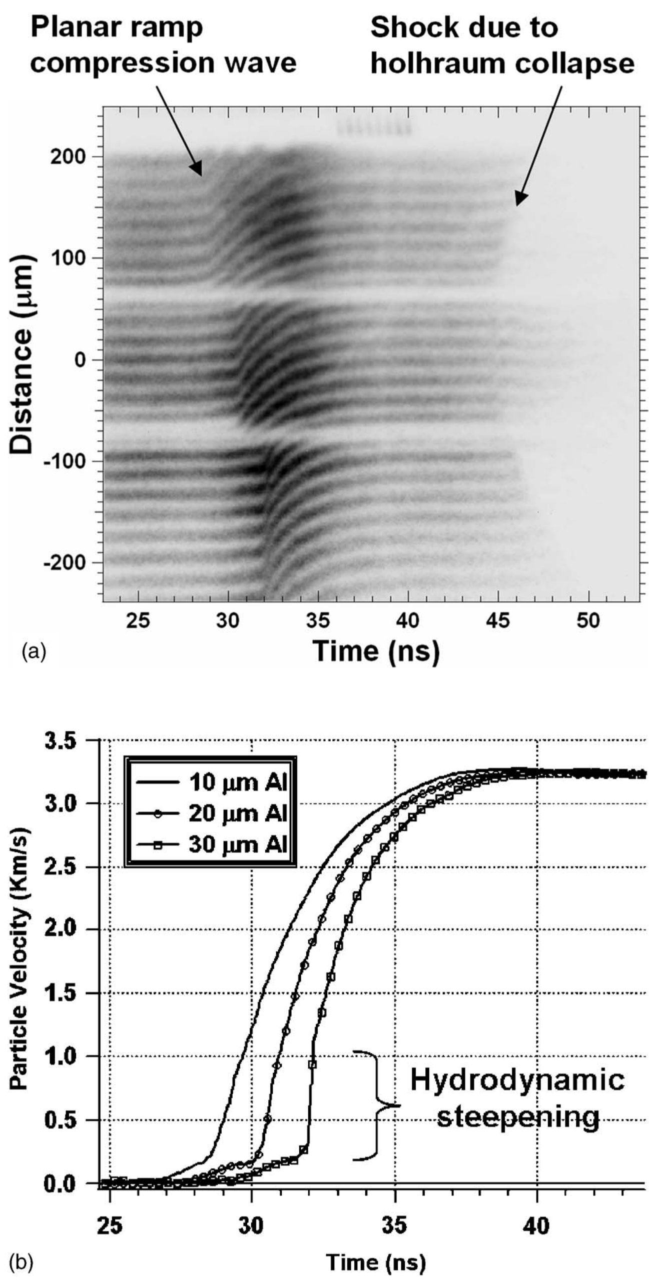

FIG. 2. (a) The output of the line imaging VISAR as recorded by an optical streak camera for an input E_{laser} of 4.5 kJ. The velocity per fringe is 1.105 km s^{-1}. Excellent planarity (Δtime/time$\sim$0.2%) is observed over the $\sim$500 μm field of view. A late time spherical shock, associated with the halfraum collapse, reaches the Al/LiF interface $\sim$15 ns after the peak of the ramp-compression-wave. (b) Al/LiF particle velocity profiles are extracted as a function of time for the 10, 20, and 30 μm steps.

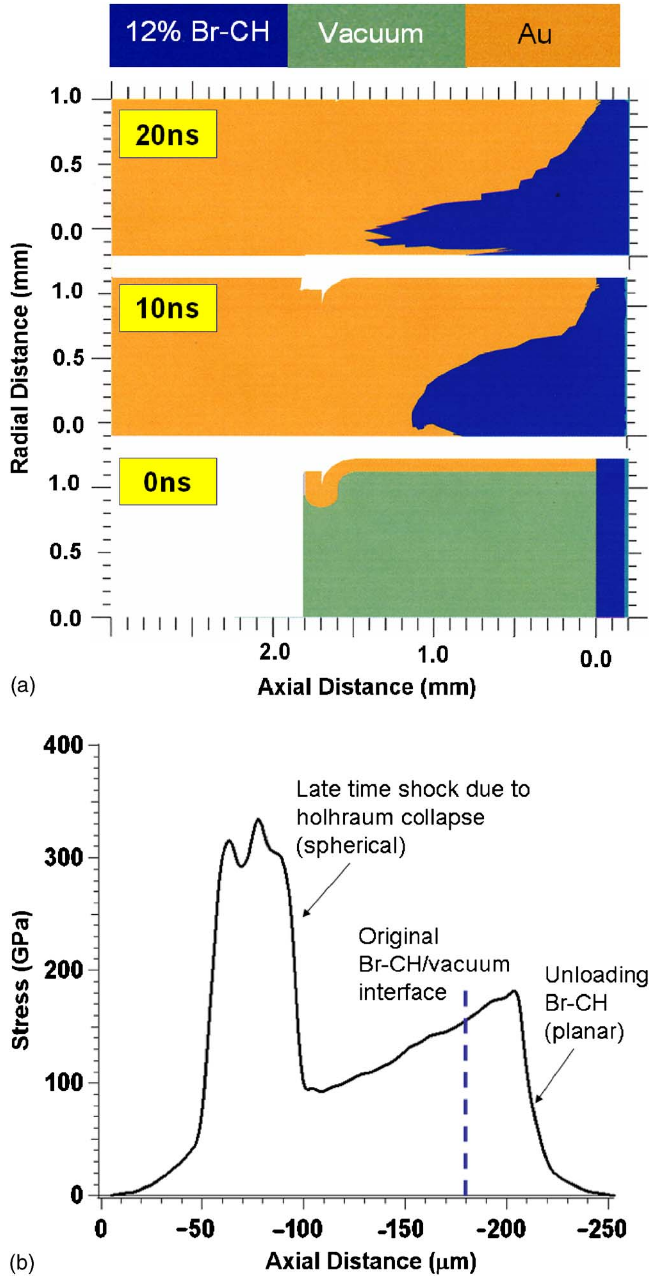

FIG. 3. (Color online) (a) Two-dimensional Lasnex simulations for the target conditions described in Fig. 1 predict that on-axis convergence of ablated Au holhraum wall material occurs at $\sim t_0+10-15$ ns. This results in a rapid increase in localized density and temperature which radiatively couples to the target launching a late-time spherical shock on axis. (b) Stress as a function of distance relative to the front of the 180 μm Br-CH reservoir at t_0+20 ns, for the target and irradiation conditions described in Fig. 1.

t_0. T_{rad} peaks at $\sim t_0+2$ ns as the laser radiation turns off. The Au material ablated normally from the halfraum walls cylindrically converges on-axis between 10 and 15 ns after t_0. This process is tamped somewhat by the ablated Br-CH reservoir material streaming into the halfraum cavity. As the Au stagnates, it creates a spike in density and temperature which radiatively couples to the Br-CH launching a late-time-shock along the target axis. As the source of this shock is localized along the halfraum axis the shock-front propagates in a spherical fashion.

By postprocessing the output files, we obtained the x-ray flux hitting the back wall of the halfraum, where the Br-CH reservoir sits. This time-resolved and spectral-energy-resolved x-ray flux then drives a 1D finely zoned simulation of the reservoir and target. This simulation provides stress and velocity as a function of time that can be compared to experimental data. Shown in Fig. 3(b) is the predicted P_x profile as a function of distance from the original front surface of the Br-CH material (ablation surface) at t_0+20 ns. The primary compressive shock, launched at t_0, hydrodynamically decays into a blast-wave before exiting the rear surface of the reservoir. As the material unloads across the vacuum gap the density gradient associated with the stress front relaxes. For larger vacuum gaps the peak P_x drops and the density gradients continue to soften. The late-time (spherical) shock caused by the halfraum collapse is predicted by the simulations and observed in the data record on the VISAR. The collapse of the halfraum may be delayed (and the region of planarity increased) by increasing the halfraum diameter although a larger laser energy input would be required to maintain a given T_{rad}.

C. Drive planarity

As shown in Fig. 2(a) excellent drive planarity across the field of view is observed with smooth ramp-unloading from the 10, 20, and 30 μm Al samples at progressively later times. However, the raw VISAR data contains spatial and temporal nonlinearities due to the configuration of the electron focusing optics within the optical streak camera. To ascertain the planarity of the pressure drive it was necessary to quantify this distortion map and then linearize the time-space scales on the data images. To generate a distortion map we splayed the time fiducials [seen in Fig. 2(a) at the top of the screen] across the entrance slit of the streak camera. Each time pulse then revealed the true shape of the time contour for a given region of the output screen. The temporal separation between the eight 60 ps timing pulses was determined precisely to be 0.548 ns with a fast detector and a spectrum analyzer. The spatial and temporal nonlinearities were warped onto a linear grid with a mesh-warping algorithm.[21] The separation between time contours allowed for calibration of the sweep speed at each point along the slit (distance axis). The timing fiducials in Fig. 2(a) appear sloped in time as the distortion map did not extend to this region of the data record. After obtaining the full velocity history at each point in space on the distortion corrected data images the spatial planarity of the drive is defined as the distribution of the time of arrival for a given velocity contour or Δtime/time. Analyzing each step in Fig. 2 and for different velocity contours gives a Δtime/time planarity of ~0.2% over the 500 μm full field of view. Nonplanarities in this drive may result from target thickness variations, spatial gradients in T_{rad} within the halfraum or, perhaps, Rayleigh-Taylor instabilities as the low density unloading plasma from the reservoir loads up against the solid aluminum target.

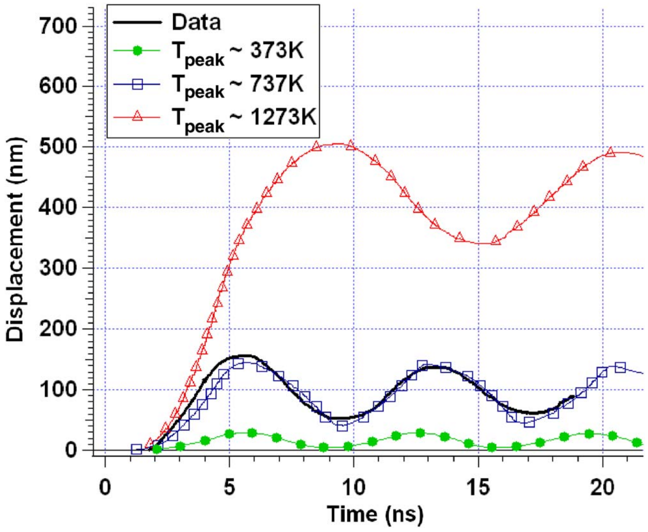

FIG. 4. (Color online) Displacement of a 25 μm thick aluminum foil due to thermal expansion after absorption of x rays generated within the halfraum. In this experiment a 2% Br-CH foil was used instead of the standard 12% Br-CH foil. Also shown are fits to the data for peak heating temperatures of 373 K, 737 K, and 1273 K.

D. Preheat

In order to obtain data on the material response it is important to have accurate knowledge of the temperature and density of the target. X rays produced in the halfraum may directly penetrate through the target package and preheat the stepped Al target. The spectral content of x rays emitted from the halfraum is well understood by many previous investigations. In the experiments reported here the potential for x-ray preheat stems from Au M band emission (2–5 keV) and above. In this spectral range the cold opacity for the 180 μm 12% Br/CH foil used as a heat shield gives an attenuation of $\sim 10^{-35}$ (2 keV) to 0.01(6 keV). In an attempt to quantify the level of preheat experimentally we replace the 12% Br-CH foil with a 2% Br-CH foil ($C_{25}H_{24}Br_2$) which gives a lower attenuation of $\sim 10^{-9}$–0.36 over the 2–6 keV spectral range. In the target design in Fig. 1 we replaced the Al/LiF target with a 25 μm Al free-standing foil. As the laser radiation turns on, x rays penetrate through the low dopant Br-CH foil and are absorbed by the Al foil. Using the VISAR as a diagnostic we observed instantaneous thermal expansion of the Al foil to a peak velocity of 60 m/s followed by contraction due to the material strength. This oscillation was repeated over the duration of the measurement. Integrating under the velocity profile a displacement of the Al foil-vacuum interface is determined and shown in Fig. 4. Based on the calculated spectral content/output flux of the source and the cold opacity of the 2% Br-CH foil, the expected spectral region to dominate the preheat is ~4–6 keV. Over this energy range the average optical depth in aluminum is 25 μm. Using a 1D hydrocode coupled to an equation-of-state for aluminum the front surface of the 25 μm foil was driven to a peak temperature, T_{peak}, for the 2 ns over which the laser irradiation is on. This corresponds to the time over which the flux associated with the higher photon energies are at a maximum. For the estimated optical depth of 25 μm, T_{peak} was varied and the resultant displacement was compared against experimental observations. Calculated displacements for T_{peak} of 373, 737, and 1237 K are shown alongside the experimental data in Fig. 4. Using this analysis we estimate a T_{peak} of ~737 K when a 2% Br/CH foil is used. A more rigorous test of this technique would utilize multistepped aluminum samples. The estimated flux transmitted through 12% Br-CH would be insufficient to preheat the target by more than several degrees.

In addition, there is strong heating due to the unloading plasma stagnating upon the Al target. As the Br-CH recompresses there is a rapid temperature increase as the ramp-compression-wave is launched. To quantify the magnitude and relative timing of the resultant heat wave, the thermal emission from the target was imaged onto the entrance slit of

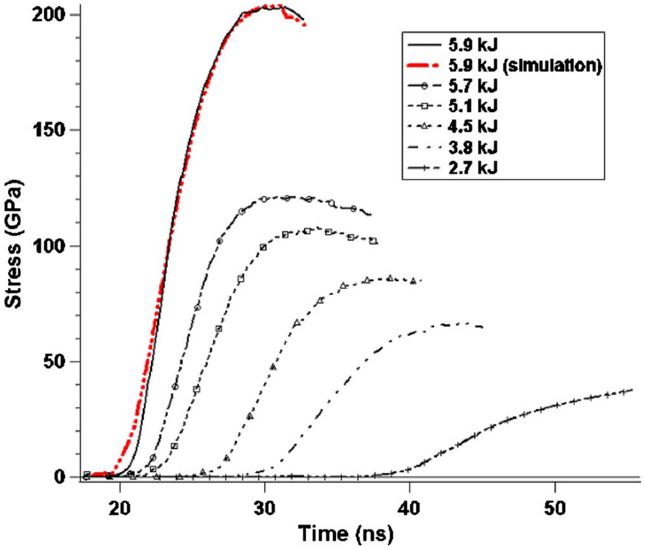

FIG. 5. (Color online) The time resolved stress source is calculated via a back-integration technique (Ref. 23). A family of loading profiles are shown as a function of input laser energy. An increase in energy results in an increase in $T_{\rm rad}$ and therefore higher P_x in the ablatively driven shock-wave launched into the reservoir material. The shock ionized Br-CH travels at higher velocities across the vacuum-gap and the increased momentum gives rise to higher ramped peak P_x in the aluminum target with associated shorter risetimes.

a streak camera. These time-resolved pyrometry measurements (synchronized with the VISAR measurements) confirm that the diffusion of this heat-wave lags well behind the main ramp-compression wave.[22] These preheat measurements suggest that the target material remains cold before the arrival of the ramp compression wave.

III. TARGET ENERGETICS

The particle velocity history of the Al allows for the compression source to be determined by integrating the equations of motion backward in space with the EOS of aluminum, the target thickness and the time-dependent particle velocity at the rear surface as an input.[23] The applied ramp-stress waves for the target conditions described in Fig. 1 are shown in Fig. 5 for a number of input laser energies, $E_{\rm laser}$. Higher peak stresses and correspondingly shorter risetimes are achieved with increasing laser energy. An increase in $E_{\rm laser}$ results in an increase in $T_{\rm rad}$ and therefore a higher P_x in the ablatively driven shock-wave launched into the reservoir material. A higher shock P_x breakout at the rear surface of the reservoir material causes the Br-CH material to unload at higher velocities across the vacuum gap. The increased momentum gives rise to a higher peak P_x in the ramp-compression-wave with associated shorter risetimes. The data shown in Fig. 2(b) was for $E_{\rm laser}$ of ~4.5 kJ. In direct drive laser ICE,[10] rapid cooling at the ablation front results in a more rapid falloff after the peak of the ramp-compression wave in contrast to the indirect-drive technique described here where the halfraum heat source decays more slowly. Below a certain $E_{\rm laser}$ (low $T_{\rm rad}$), the heating associated with the ablatively driven shock will not be sufficient to ionize the reservoir material. In this case, the material unloads across the vacuum-gap in clumps and a secondary ramp drive will not be launched. This sets a lower peak P_x limit in the ramp-compression wave (expected to be ~10 GPa).

TABLE I. For the target geometry described in Fig. 1, and for a range of input laser energies ($E_{\rm laser}$), the measured peak halfraum radiation temperature ($T_{\rm rad}$), peak longitudinal stress in the sample ($P_{x(\rm peak)}$), target material and thickness, ramp breakout time ($\tau_{\rm ramp}$), ramp risetime ($\Delta\tau$) and shock breakout time ($\tau_{\rm shock}$) are recorded. For shot No. s38964 a 20 μm Be ablator was glued onto the halfraum side of the Br-CH reservoir and a 600 μm vacuum gap was used.

Shot No.	$E_{\rm laser}$ (kJ)	Target	$P_{x(\rm peak)}$ (GPa)	$T_{\rm rad}$ (eV)	$\tau_{\rm ramp}$ (ns)	$\Delta\tau_{\rm ramp[10\%-90\%]}$ (ns)	$\tau_{\rm shock}$ (ns)
s39720	2.25	20 μm Al	26	104.9	43	>14.5	57.5
s39723	2.65	55 μm Al	31	108.8	46.6	>9.4	66.4
s40125	3.5	65 μm Al	52	117.1	42.6	>12.9	55.5
s40126	3.8	20 μm Al	64	126.0	33.2	6.5	48.2
s40127	4.5	⋯	84	128.7	29.6	5.27	44.6
s38962	5.08	⋯	98	132.3	26.2	4.26	44.2
s38963	5.42	⋯	110	134.8	25.2	3.59	41.8
s38961	5.7	⋯	120	134.0	25	3.3	⋯
s38964[a]	5.93	6 μm Al	210	137.8	21.7	4.82	⋯

[a] Target had a Be ablator and a 600 μm vacuum gap.

The highest peak longitudinal stress is achieved for a $E_{\rm laser}$ of 5.9 kJ. For this particular shot a 20 μm Be ablator was glued onto the halfraum side of the Br-CH reservoir and a 600 μm vacuum-gap was used. Be has a higher ablation velocity than the 12% Br-CH and so for a fixed input energy a higher $P_{x(\rm peak)}$ is achieved. This target and irradiation geometry has been simulated with LASNEX with good agreement to the experimentally determined stress source (Fig. 5). A summary of experimental observables are listed in Table I for the target configuration described in Fig. 1 and for a range of $E_{\rm laser}$. Increasing $E_{\rm laser}$ from 2.3 kJ to 5.7 kJ, increases $P_{x(\rm peak)}$ from 21 GPa to 120 GPa. This is driven by the approximately linearly increase in $T_{\rm rad}$ from 105 eV to 134 eV. In these experiments $T_{\rm rad}$ is measured with a Dante spectrometer[15] with a 70° viewing angle to the LEH. This oblique viewing angle makes the $T_{\rm rad}$ calculation more sensitive to LEH closure and introduces an estimated uncertainty of ~5 eV in the measurement. For all $E_{\rm laser}$ the late time shock is observed 10–20 ns after the onset of the ramp-wave. For $P_{x(\rm peak)} \gtrsim 55$ GPa the ramp waves have reached a peak before the arrival of the late time shock. In these cases EOS measurements, which are made up to the peak of the ramp-unloading-wave, would be unaffected. For $P_{x(\rm peak)} \lesssim 55$ GPa however the risetime of the ramp-wave has increased such that the late time shock cuts off the ramp-wave before it has reached a peak. For $P_{x(\rm peak)}$ of 26 GPa the risetime of the ramp-wave $\Delta t_{\rm ramp}$ is >15 ns (truncated by late-time shock) whereas for a $P_{x(\rm peak)}$ of 120 GPa, $\Delta t_{\rm ramp}$ is 3.3 ns. The shock-up distance is shorter for shots with higher $P_{x(\rm peak)}$.

IV. CONCLUSIONS

We have demonstrated a technique for generating a high planarity (~0.2%) ramp compression over a several hundred micron region, by converting spatially inhomogeneous laser radiation into a spatially uniform temperature x-ray drive. This ensures an identical ramped-stress wave is applied simultaneously to the loading surface of a stepped Al sample. The use of a 12% Br-CH foil has been shown to be an effective heat-shield from energetic x rays produced in the halfraum which could otherwise preheat the target. Using the x-ray drive technique described here, single shot equation-of-state data close to the room temperature isentrope of pure Al has been extracted up to 110 GPa.[24] Designs predict that we will be able to extend this quasi-isentropic compression technique to above 1000 GPa on NIF.[1]

ACKNOWLEDGMENTS

The authors would like to thank Albert Osterheld for his continued support of this work. We would also like to thank Ralph Page and Klaus Widmann for analyzing the Dante spectrometer data.

This work was performed under the auspices of the U.S. Department of Energy by the University of California, Lawrence Livermore National Laboratory under Contract No. W-7405-Eng-48.

[1] M. J. Edwards, K. T. Lorenz, B. A. Remington, S. Pollaine, J. Colvin, D. Braun, B. F. Lasinski, D. Reisman, J. M. McNaney, J. A. Greenough, R. Wallace, H. Louis, and D. Kalantar, Phys. Rev. Lett. **92**, 075002 (2004).

[2] R. S. Hawke, D. E. Duerre, J. G. Huebel, H. Klapper, and D. J. Steinberg, J. Appl. Phys. **43**, 2734 (1972); J. R. Asay, AIP Conf. Proc. **505**, 261 (2000).

[3] J. R. Asay, Int. J. Impact Eng. **20**, 27 (1997).

[4] J. F. Barnes, P. J. Blewett, R. G. McQueen, K. A. Meyer, and D. Venable, J. Appl. Phys. **45**, 727 (1974).

[5] For a review, see R. F. Trunin, *Shock Compression of Condensed Materials* (Cambridge University Press, Cambridge, 1998).

[6] A. D. Chijioke, W. J. Nellis, and I. F. Silvera, J. Appl. Phys. **98**, 073526 (2005).

[7] S. D. Rothman, J-P Davis, J. Maw, C. M. Robinson, K. Parker, and J. Palmer, J. Phys. D **38**, 733 (2005).

[8] J-P. Davis, J. Appl. Phys. **99**, 103512 (2006).

[9] K. T. Lorenz, M. J. Edwards, S. G. Glendinning, A. F. Jankowski, J. McNaney, S. M. Pollaine, and B. A. Remington, Phys. Plasmas **12**, 056309 (2005).

[10] K. T. Lorenz, M. J. Edwards, A. F. Jankowski, S. M. Pollaine, R. F. Smith, and B. A. Remington, High energy density physics **2**, 113 (2006).

[11] S. D. Rothman, A. M. Evans, P. Graham, C. J. Horsfield, and T. Jalinaud, J. Phys. D **35**, 3021 (2002).

[12] S. D. Rothman, A. M. Evans, C. J. Horsfield, P. Graham, and B. R. Thomas, Phys. Plasmas **9**, 1721 (2002).

[13] Laboratory of Laser Energetics, University of Rochester, New York.

[14] For a review see, J. D. Lindl, *Inertial Confinement Fusion: The Quest for Ignition and Energy Gain Using Indirect Drive* (Springer-Verlag, New York, 1998).

[15] C. Sorce, J. Schein, F. Weber, K. Widmann, K. Campbell, E. Dewald, R. Turner, O. Landen, K. Jacoby, P. Torres, and D. Pellinen, Rev. Sci. Instrum. **77**, 10E518 (2006).

[16] P. M. Celliers, D. K. Bradley, G. W. Collins, D. G. Hicks, T. R. Boehly, W. J. Armstrong, Rev. Sci. Instrum. **75**, 4916 (2004).

[17] J. L. Wise and L. C. Chhabildas, *Shock-Waves in Condensed Matter–1985*, edited by Y. M. Gupta (Plenum, New York, 1986), pp. 441–454.

[18] H. Huang and J. R. Asay, J. Appl. Phys. **98**, 033524 (2005).

[19] R. F. Smith, K. T. Lorenz, D. Ho, B. A. Remington, A. Hamza, J. Rogers, S. M. Pollaine, S. Jeon, Y-S. Nam, and J. Kilkenny, Astrophys. Space Sci. **307**, 269 (2007).

[20] G. B. Zimmerman and W. L. Kruer, Comments Plasma Phys. Controlled Fusion **2**, 51 (1975).

[21] D. B. Smythe, "A two-pass mesh warping algorithm for object transformation and image interpolation" ILM Technical Memo No. 1030, Computer Graphics Department, Lucasfilm Ltd., 1990.

[22] H-S. Park, "Diagnoses of target preheat in laser driven quasi-isentropic compression experiments" (unpublished).

[23] D. B. Hayes, C. A. Hall, J. R. Asay, and M. D. Knudson, J. Appl. Phys. **94**, 2331 (2003), and references within.

[24] R. F. Smith, J. H. Eggert, A. F. Jankowski, P. M. Celliers, M. J. Edwards, Y. M. Gupta, J. R. Asay, and G. W. Collins, Phys. Rev. Lett. **98**, 065701 (2007).